ACS APPLIED MATERIALS & INTERFACES

Research Article

www.acsami.org

Synergistic Effects of Self-Doped Nanostructures as Charge Trapping Elements in Organic Field Effect Transistor Memory

Haifeng Ling,[†,⊥] Jinyi Lin,[‡,⊥] Mingdong Yi,[*,†] Bin Liu,[†] Wen Li,[†] Zongqiong Lin,[‡] Linghai Xie,[*,†] Yan Bao,[†] Fengning Guo,[†] and Wei Huang[*,†,‡]

[†]Center for Molecular Systems and Organic Devices (CMSOD), Key Laboratory for Organic Electronics and Information Displays & Institute of Advanced Materials (IAM), Jiangsu National Synergetic Innovation Center for Advanced Materials (SICAM), Nanjing University of Posts & Telecommunications (NUPT), 9 Wenyuan Road, Nanjing 210023, China

[‡]Key Laboratory of Flexible Electronics (KLOFE) & Institute of Advanced Materials (IAM), Jiangsu National Synergetic Innovation Center for Advanced Materials (SICAM), Nanjing Tech University (NanjingTech), 30 South Puzhu Road, Nanjing 211816, China

Supporting Information

ABSTRACT: Despite remarkable advances in the development of organic field-effect transistor (OFET) memories over recent years, the charge trapping elements remain confined to the critical electrets of polymers, nanoparticles, or ferroelectrics. Nevertheless, rare reports are available on the complementary advantages of different types of trapping elements integrated in one single OFET memory. To address this issue, we fabricated two kinds of pentacene-based OFET memories with solution-processed amorphous and β-phase poly(9,9-dioctylfluorene) (PFO) films as charge trapping layers, respectively. Compared to the amorphous film, the β-PFO film has self-doped nanostructures (20−120 nm) and could act as natural charge trapping elements, demonstrating the synergistic effects of combining both merits of polymer and nanoparticles into one electret. Consequently, the OFET memory with β-PFO showed nearly 26% increment in the storage capacity and a pronounced memory window of ∼45 V in 20 ms programming time. Besides, the retention time of β-PFO device extended 2 times to maintain an ON/OFF current ratio of 10^3, indicating high bias-stress reliability. Furthermore, the β-PFO device demonstrated good photosensitivity in the 430−700 nm range, which was attributed to the additive effect of smaller bandgap and self-doped nanostructures of β-phase. In this regard, the tuning of molecular conformation and aggregation in a polymer electret is an effective strategy to obtain a high performance OFET memory.

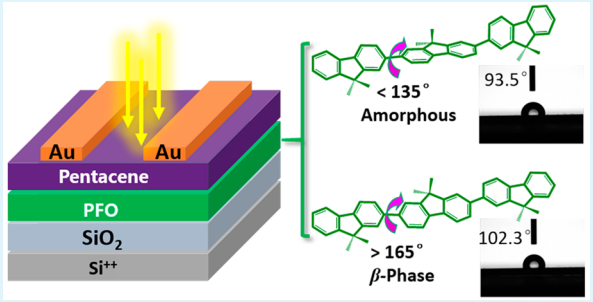

KEYWORDS: *OFET memory, polymer, conformation, β-phase, nanostructure*

INTRODUCTION

Nonvolatile organic field-effect transistor (OFET) memories have received extensive attention for their light weight, structural flexibility, nondestructive readout, and multibit storage in a single cell.[1−4] Up to date, a variety of multifunctional charge storage elements (referred to electrets) have been developed to improve the charge trapping density and stability, which generally can be categorized into three types: polymers,[1,5] nanoparticles (NPs),[6,7] and ferroelectrics.[8,9] However, in most instances, the above trapping elements were always used independently and did not realize the complementary advantages. Recently, a double floating-gate strategy has been proposed to adopt different metal NPs or two-dimensional (2D) nanoflakes simultaneously in one nano-floating gate OFET memory.[10−13] Nevertheless, the memory performances are unavoidably influenced by the NPs size and distribution, which were limited to the thermal evaporation process or the hybrid concentration.[14,15] Thereby, many attempts have been made on the simple solution-processed polymer electrets.[16,17] Previous studies revealed that electronic and topological structure of polymer, such as p−n electronic structure, limited effective conjugated length, and unique steric interaction are closely associated with the tuning of memory characteristics.[1,3,18] But beyond that, polymer chains process supramolecular interaction and topological structure and tend to stack one by one and then assemble into nanostructures or aggregates which may act as self-doped charge trapping elements for memories. In addition, it is found that through light-assisted programming the charge trapping capacity of OFET memories can be further improved.[19−21] In view of the above facts, however, a photosensitive electret that integrates both merits of polymer and NPs has yet to be announced.

In this regard, polyfluorenes (PFs) are a promising candidate with various nano- or microstructures to satisfy the aforementioned requirements.[22,23] Among them, β-phase, which stemmed from an intriguing "planar zigzag" (2_1 helix)

Received: March 30, 2016
Accepted: July 1, 2016

DOI: 10.1021/acsami.6b03792
ACS Appl. Mater. Interfaces XXXX, XXX, XXX−XXX

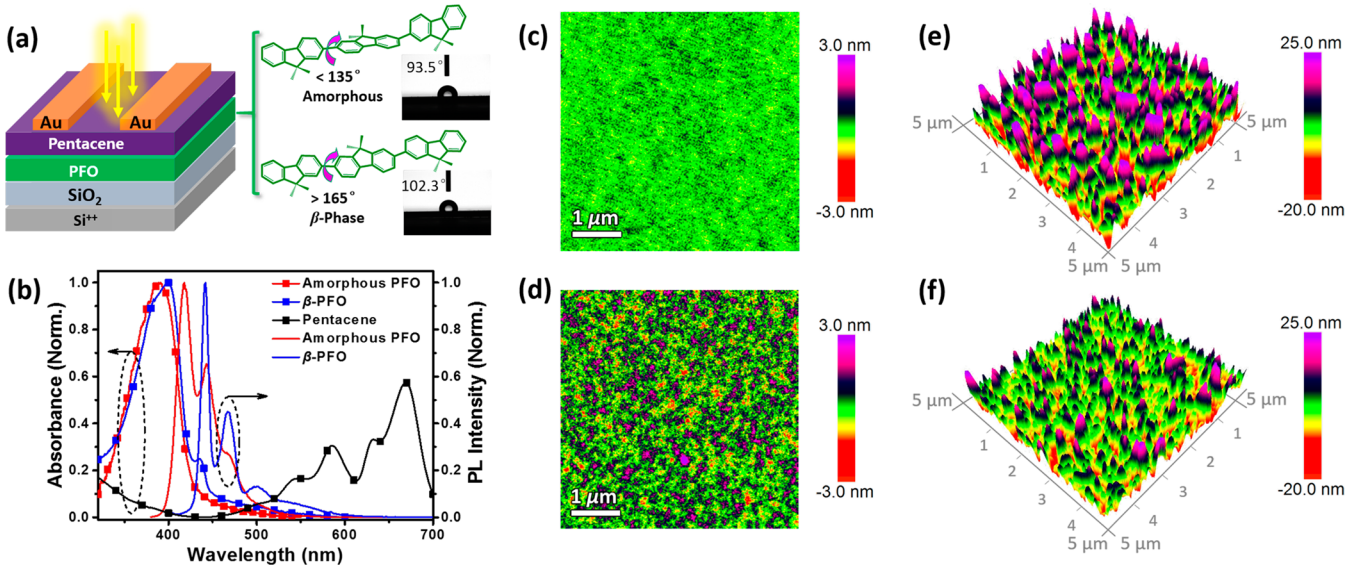

Figure 1. (a) Schematic configuration of the pentacene-based OFET memory device with amorphous or β-PFO film as electrets, together with the water contact angles of the PFO surface (side view of a drop of water). (b) UV–vis absorption spectra of amorphous PFO, β-PFO, and pentacene films (left axis). PL spectra of amorphous and β-PFO films (right axis). 2D AFM images of (c) amorphous PFO film and (d) β-PFO film. Corresponding 3D AFM images of 40 nm thick pentacene deposited on (e) amorphous PFO film and (f) β-PFO film.

chain conformation, showed higher current efficiency (CE) and electroluminescence (EL) spectral stability in deep blue polymer light-emitting diodes (PLEDs).[24] Such a high efficiency results from the critical functionalities of the β-phase: electron-trapping and promoted hole mobility (10^{-5} cm^2 V^{-1} s^{-1}),[25] which indicates the β-phase may potentially serve as charge trapping elements in OFET memories.[26,27] Previously, Feng et al. reported nanostructured PFO (10–15 nm) dispersing in poly(methyl methacrylate) (PMMA) and modulated the threshold voltage (V_{th}) under light illumination.[27] Shih et al. demonstrated 50–70 nm PFO NPs embedded into poly(methacrylic acid) (PMAA) to construct a molecular level nanofloating gate OFET memory.[26] However, the formation of β-phase in film state correlated charge trapping mechanism for OFET memory is still unclear.

In this work, we fabricated pentacene-based OFET memories with β-PFO and amorphous PFO films as charge trapping elements to clarify the β-phase effect on the OFET memory characteristics. UV–visible (UV–vis) absorption and photoluminescence (PL) spectra were employed to confirm the formation of β-phase in the film states. The morphology influence of β-phase was studied by atomic force microscopy (AFM) and contact angle measurements. OFET memory properties including hysteresis windows (with and without illumination), light-assisted reversible threshold voltage shifts, and endurance performances were investigated, suggesting the β-PFO device showed better memory performances and photosensitivity than the amorphous one. The corresponding mechanism of β-phase on the trapping of hole and electron in OFET memory was detailedly discussed. Finally, we further investigated the effect of β-phase content on the charge trapping behavior.

EXPERIMENTAL SECTION

Fabrication of OFET Memories. Figure 1a shows the schematic illustration of the OFET memories with a top-contact and bottom-gate configuration. Heavily doped n-type Si wafer with 300 nm SiO_2 was used as the substrate. The substrate was cleaned sequentially in an ultrasonic bath with acetone, ethanol, and deionized water for 10 min each and then dried in the oven at 120 °C for 30 min. Later, the substrate surface was UV/ozone cleaned for 3 min and transferred to a N_2-filled glovebox. Next, about 60 nm thick PFO films were spin-coated from a 5 mg/mL chloroform solution and then baked at 50 and 80 °C separately on a hot plate for 30 min to remove the residual solvent. Two types of PFO films, namely amorphous PFO baked at 50 °C and β-PFO baked at 80 °C, were used to create the electret layers. After that, 40 nm thick pentacene was thermally evaporated at a deposition rate of 0.1 Å s^{-1} under a pressure of 5×10^{-4} Pa. Finally, about 50 nm thick Au was thermally evaporated through a shadow mask to form source and drain electrodes with the channel width W = 2000 μm and length L = 100 μm. Besides, control devices with (octadecyltrichlorosilane) OTS gate dielectric treatment were also fabricated.

Characterizations. UV–vis absorption spectra were measured with a Shimadzu UV-3600 spectrometer at room temperature, and PL spectra were recorded on a Shimadzu RF-5301(PC) luminescence spectrometer. The film morphologies of PFO and pentacene films were recorded with a Bruker's Dimension Icon AFM in tapping mode (Bruker's Sb/Si probe tip with a resonant frequency 320 kHz and the spring constant 42 N m^{-1}). Commercial LED with a wavelength of 410–800 nm (visible-light spectroscopy, see Figure S1) was shined directly from the top of the device with an intensity of 5 mW cm^{-2}. The electrical characteristics were measured by an Agilent B1500A semiconductor parameter analyzer in a shielding box and in ambient air, and the thicknesses of PFO films were measured using a Bruker Dektak XT stylus profiler. A two liquid (water and diiodomethane) contact angle method was adopted to explore the surface energy (γ_S) of PFO on SiO_2 substrate (see Supporting Information for the details).

RESULTS AND DISCUSSION

Optical Properties of Amorphous and β-Phase PFO Films. UV–vis absorption and PL spectra are introduced to characterize the formation of β-phase, as shown in Figure 1b. The maximum absorption peak of PFO films by annealing at 50 °C was located at 385 nm, and its maximum emission peak was at 424 nm, indicating that the PFO films at lower annealing temperature (50 °C) was in amorphous state. However, a new absorption peak appeared at 437 nm at higher annealing temperature (80 °C); moreover, its PL spectrum was red-

DOI: 10.1021/acsami.6b03792
ACS Appl. Mater. Interfaces XXXX, XXX, XXX–XXX

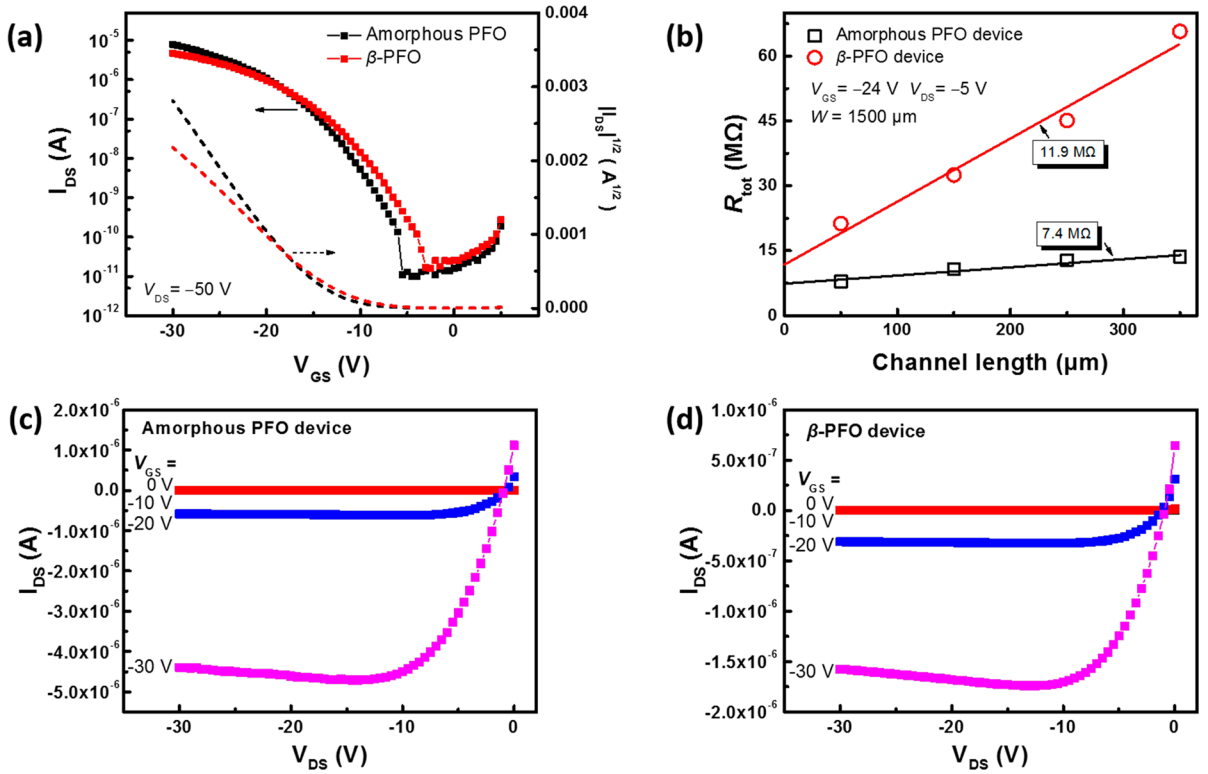

Figure 2. (a) Transfer characteristics in the linear regime (W = 2000 μm, L = 100 μm, 300 K). (b) Transfer line method (TLM) plots of pentacene-based OFET memory devices with amorphous and β-phase PFO electrets. (c) Output characteristics with amorphous PFO electret. (d) Output characteristics with β-PFO electret.

Table 1. Transistor and Memory Performances of Pentacene-Based OFET Memories with Two PFO Electrets

electret	μ_{ave} ($cm^2/(V\ s)$)	V_{th} (V)	I_{ON}/I_{OFF}	memory window (V)	Δn (cm^{-2})
amorphous	0.27 ± 0.07	−5.0 ± 0.8	7.17×10^5	45.3	2.6×10^{12}
β-phase	0.13 ± 0.04	−11.7 ± 0.03	2.78×10^5	57.0	3.3×10^{12}

shifted from 424 to 440 nm, suggesting the formation of β-phase in the film state, which was consistent with our previous reports.[24,28] In this regard, similar to PFO β-phase-based solvent-induced pattern,[22] nanostructures generated from β-phase PFO behave like a "guest", together with amorphous chain of polyfluorenes as a "host", suggesting the self-doped nanostructures in β-PFO film act as a perfect complementary system of polymer and floated nanoparticles in one electret.

Morphology and Surface Energy of PFO Films. For OFETs, the morphology and surface energy of the polymer electrets are critical factors to influence the growth and crystallinity of overlaying semiconductor (pentacene in this work).[29] In this case, we characterized the surface hydrophobicity and calculated the surface energy (γ_S) of PFO layers, as shown in the inset of Figure 1a and Table S1. The surface energy, including the polar component (γ_S^p) which is attributed to polar forces arising from permanent and induced dipoles (as well as hydrogen bonding), whereas the dispersion component (γ_S^d) is due to instantaneous dipole moments.[30] The surface polarity χ_P (i.e., the ratio of the polar component to the total surface energy) of β-phase PFO is 5.4×10^{-5} and much smaller than that of amorphous PFO (0.016), indicating that the surface of β-phase PFO interacts more weakly with water molecules. Although the presence of nanostructures can improve the film hydrophobic property from 93.5° of amorphous PFO to 102.3° of the β-PFO, the two PFO films possessed similar surface energies of 37−38 mJ/m^2 due to the high ratio of γ_S^d and would lead to a "layer + island" growth mode of pentacene.[31] Further, the 2D AFM image was used to analyze the morphology of PFO films. As shown in Figures 1c and 1d, one can see that the amorphous PFO film is quite uniform and smooth with a small root-mean-square (RMS) roughness value R_q = 0.33 nm. Conversely, β-PFO film shows rough morphology (R_q = 0.67 nm) and significant surface fluctuation (−2 to 2 nm) due to the formation of β-phase nanostructures with the size of 20−120 nm, indicating the β-PFO film could offer significant nucleation sites when pentacene deposited. Therefore, the differences of growth and crystallinity of pentacene on the two PFO films should be dominantly dependent on morphologies. As can be seen in Figures 1e and 1f, the representative 3-dimensional (3D) AFM image of pentacene on β-PFO film displayed smaller and compact pentacene grains of 0.2 μm, unlike that on amorphous PFO film with larger grains (0.41 μm) but clear grain vacancies. Moreover, due to the rough surface of β-phase PFO film, the activation energies for pentacene nucleation and re-evaporation from PFO surface were dramatically reduced during the thermal evaporation process.[32,33] Compared with the pentacene/amorphous interface, the coverage of pentacene film was better thus a larger interfacial contact area was formed between the initial growth of pentacene (ca. 1.5−5 nm, referring to the conductive channel) and β-PFO film, as depicted in Figure S2.

DOI: 10.1021/acsami.6b03792
ACS Appl. Mater. Interfaces XXXX, XXX, XXX−XXX

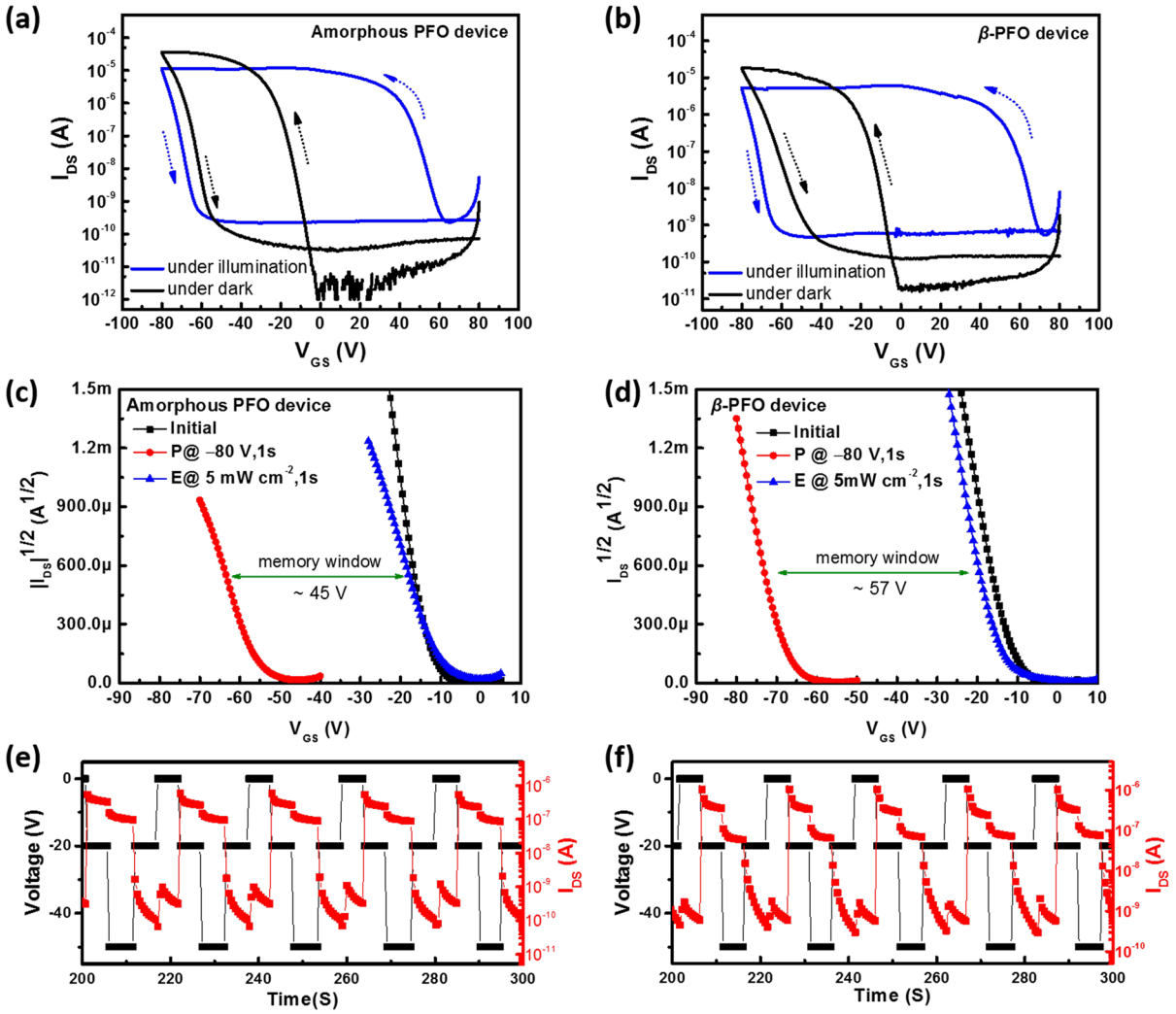

Figure 3. Dual-sweep transfer curves taken under dark (dark line) and illumination (5 mW/cm^2, blue line) of (a) amorphous PFO device and (b) β-PFO device. Reversible shifts in V_{th} (square root of I_{DS} vs V_{GS}) of (c) amorphous PFO device and (d) β-PFO device. WRER cycles of (e) amorphous PFO device and (f) β-PFO device. The drain current was measured at V_{DS} = −50 V. The writing, reading, and erasing voltages were at V_{GS} = −50, −20, and 0 V (LED light), respectively.

Electrical Characterizations of Pentacene-Based OFET Memories with PFO Films. Figure 2 shows the representative transfer and output characteristics of the pentacene-based OFET memories with the two type PFO electrets, and the calculated transistor corrected parameters are summarized in Table 1. The typical *p*-type field-effect transistor behavior with a typical linear/saturation property was observed for both of the PFO memory devices. The β-PFO device has lower mobility of 0.13 ± 0.04 cm^2 V^{-1} s^{-1} than those of amorphous PFO device (0.27 ± 0.07 cm^2 V^{-1} s^{-1}). The smaller pentacene grains in the β-PFO device were responsible for its lower mobility. Meanwhile, the smaller pentacene grains induced a larger contact resistance (R_c) of 11.9 MΩ at the Au/pentacene contact (Figure 2b), which would lower the extraction of the mobility. Besides, the rough channel region (pentacene/β-PFO interface) could also influence the carrier transporting due to charge scattering effect.[34]

To investigate the impact of self-doped nanostructures on the memory properties, the hysteresis window of the transfer curve upon double sweeping was measured, as illustrated in Figures 3a and 3b. The double sweeping of V_{GS} was from 80 to −80 V and then backward under dark and light conditions, respectively. Both of the memories show obvious counter-clockwise hysteresis loops. For the amorphous PFO device, the hysteresis window was approximately 50 V (31% of the total applied bias) under dark and mainly located in the negative V_{GS} region, indicating that the trapped charges were holes. Under illumination, the hysteresis window was extended to ∼126 V (78% of the total applied bias) and located in bipolar V_{GS} region, demonstrating both holes and electrons could be trapped with light assistance as we previously reported.[19] By contrast, the β-PFO device processed larger hysteresis window either under dark (∼54 V) or under illumination (∼140 V), exhibiting the β-PFO device has pronounced electron trapping capacity under illumination. It should be noted that there are some other physical factors that can cause hysteresis in OFETs, such as polarization of dipolar groups (e.g., −OH) in the electret bulk, water absorbance induced traps within the semiconductor or at the semiconductor/electret interface, and charges injected from gate electrode.[35−37] Considering that there is no −OH group in PFO chain, the influence of polarization in PFO bulk can be excluded. Besides, thermally grown 300 nm thick SiO_2 is enough to block the charge injection from gate electrode.[35] In this regard, we remeasured

DOI: 10.1021/acsami.6b03792
ACS Appl. Mater. Interfaces XXXX, XXX, XXX−XXX

the hysteresis to check the influence of water absorbance by leaving both of the OFET memories in a constant temperature and humidity controlling box for 2 weeks (with the humidity of 30−40%). From Figure S3, one can see that the amorphous PFO device showed obvious volatile anticlockwise hysteresis, which is in agreement with the feature caused by water induced traps.[36,37] However, the hysteresis was negligible in the β-PFO device, which is attributed to the additive effects of the compact pentacene grains deposited on β-PFO and hydrophobicity of β-PFO surface. Generally, larger pentacene grains allow the water molecules to penetrate quickly and easily through the semiconductor layer and to be adsorbed at the pentacene grain boundaries and the pentacene/PFO interface.[38,39] The water molecules could generate long-lifetime electron traps, so extra holes are needed to balance the prestored electrons during the positive to negative sweeping process, created an inaccurate large hysteresis window of 50 V for amorphous PFO device under dark.[36] By comparison, the compact pentacene grains deposited on β-PFO film could help suppress the diffusion of water molecules. As a result, the damp atmosphere induced instability can be weakened in the β-PFO device, demonstrating that the formation of self-doped nanostructures is beneficial to improve the device reliability in air.

In order to better compare the hole trapping ability of the two kinds of PFO films, the reversible threshold voltage shifts were performed. As shown in Figures 3c and 3d, the programming/erasing operations were −80 V (under dark)/0 V (with light) for 1 s. When the application of V_{GS} = −80 V was applied to the device for 1 s in the dark, the transfer curve shifted toward the negative direction, serving as the programming process. Subsequently, the memory device was illuminated for 1 s, and then the transfer curve recovered to its initial state, serving as the erasing process. The memory windows between the programmed and erased states were calculated approximately 45 and 57 V for amorphous and β-PFO device, respectively. It is worth noting that the memory window of the pentacene-based OFET memories originate from the holes tunneling into the pentacene/polymer interface and polymer electret under negative V_{GS}.[3,5] In our work, the larger memory window of β-PFO device might be attributed to the stronger charge trapping ability of β-PFO induced self-doped nanostructures and the enlarged interfacial contact area between pentacene and β-PFO. As mentioned in the section of optical properties, amorphous phase and β-phase coexisted in the β-PFO film and formed the "host−guest" system. The interfaces between amorphous and β-phase could act as charge trapping sites due to the potential barrier produced by the different LUMO energy levels and physical defects,[25] ultimately to improve charge storage density compared with pure amorphous PFO.[40] In addition, the larger interfacial contact area between pentacene and β-PFO films could help broaden the effective tunneling area and ensure more charge injection.[41,42] The trapped holes played a critical role in the formation of internal electric field (E_{in}) and then blocked the subsequent hole injection.[21,43] However, the trapped holes can be released through photogenerated electrons in the light erasing process.[21,43,44] According to the equation $E = hc/\lambda$, the maximum photon energy of our incident light is calculated to be ca. 2.9 eV, which is larger than the band gap of pentacene (~1.9 eV) but extremely close to that of amorphous PFO (2.94 eV).[25] By exposing amorphous PFO device to illumination, the photoexcitons were generated mainly in pentacene and diffused toward the conductive channel to be separated by E_{in}. Then the photoexcited high-energy electrons can neutralize the trapped holes. Despite the same HOMO energy level, the LUMO level of β-PFO was 0.12 eV lower than that of amorphous PFO, thus leading to a smaller bandgap of 2.82 eV. Therefore, the β-PFO electret could increase the amount of photoexcitons and enhance the photosensitivity of pentacene-based OFET in blue light range (435−450 nm, Figure 1b).

The multiple electrical−optical switching is evaluated to further explore the effect of β-PFO on the electron trapping, with a series of programming (V_{GS} = −50 V, under dark), reading (V_{GS} = −20 V, under dark), and erasing (V_{GS} = 0 V, under illumination) processes (refer to WRER cycles). As shown in Figures 3e and 3f, both the PFO memories exhibited rewritable memory characteristics with high ON/OFF current ratio of ~10^3. It can be seen that the ON current (erased state) was stable for both of the memories during the WRER cycles (Figure S4). However, the OFF current (programmed state) of the β-PFO device showed an upward trend from 6.1×10^{-11} to 1.0×10^{-9} A in the initial cycles and then remained relatively unchanged. The initial increment in OFF current can be attributed to the electron trapping ability of β-PFO. As mentioned above, both pentacene and β-PFO film contributed to the generation of photoexcitons, and the rough contact area between the pentacene and β-PFO films could provide additional exciton-separation sites; thus, a large number of photogenerated electrons were generated in the conductive channel of the β-PFO device, making sure the full neutralization of previously trapped holes. In addition, the lower LUMO level also brought a strong electron trapping ability to localize the residue photogenerated electrons. Moreover, due to the self-doped morphology of β-PFO film, the surrounded amorphous PFO chain may act as tunneling matrix and suppress the electron release. Taking into account the promoted hole mobility of the β-PFO film (Figure S5), the negative pulse of V_{GS} = −50 V might not offer enough holes to neutralize the trapped photogenerated electrons during the fast optical−electrical switching process.[45] Thus, the trapped photogenerated electrons would become more after several light erasing operations and induce a positive V_{TH} shift of the programmed state.[45] Under the same reading voltage, OFF state current increased until the accumulation reached saturation. As a consequence, OFET memory with β-phase PFO also demonstrated well electron trapping ability.

In a sense, high hole trapping capacity represents the tunability of V_{th} for the *p*-channel OFET memories, so it is necessary to research the variation in trapped charge density (Δn) as the function of the programming voltage. The Δn is calculated according to the following equation: $\Delta n = (\Delta V_{TH}/e) C_i$, where e is the element charge, C_i is the total capacitance per unit area (roughly calculated from the equation $1/C_i = 1/C_{PFO} + 1/C_{SiO_2}$). Figure 4a shows a linear change of the ΔV_{TH} as a function of V_{GS}, corresponding to the model of Fowler−Nordheim (F−N) tunneling for charge trapping OFET memories.[44] Upon the programming voltage of V_{GS} = −80 V for 1 s, the calculated Δn was up from ca. 2.6×10^{12} cm^{-2} for amorphous PFO devices to 3.3×10^{12} cm^{-2} for β-PFO devices, reflecting that pentacene-based OFET memory with β-PFO electret has more trapping sites. The hole trapping capacity was further characterized by investigating the ΔV_{TH} as a function of applied programming time (t_{prog}) under a constant V_{GS} = −80 V. As can be seen in Figure 4b, ΔV_{TH} of both the PFO devices increased logarithmically with t_{prog} due to more trapped holes.[46]

DOI: 10.1021/acsami.6b03792
ACS Appl. Mater. Interfaces XXXX, XXX, XXX−XXX

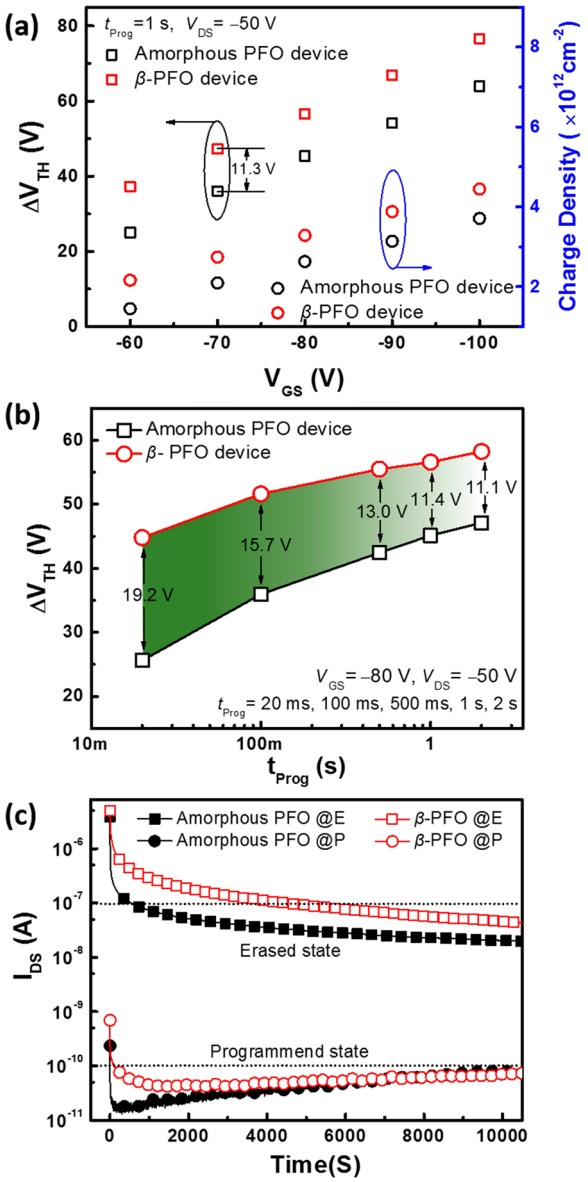

Figure 4. (a) Corresponding shifts of threshold voltage (ΔV_{TH}) and trapped charge density (Δn) as a function of negative programming bias (V_{GS}). (b) ΔV_{TH} as a function of applied programing time (t_{prog}). (c) Bias stress characteristics measured at V_{DS} = −50 V and V_{GS} = −25 V at 1 s interval.

However, the β-PFO device still processed larger memory window of 44.8 V than amorphous one (25.6 V) even in t_{prog} = 20 ms. When t_{prog} was longer (e.g., 2 s), ΔV_{TH} reached certain saturated values since the previously trapped holes will build the internal electric field.[21,43] Then the difference of memory windows between the two PFO devices got smaller and tended to be constant (~11 V). This result indicated that there existed stronger trapping sites in the β-PFO device, especially at the pentacene/β-PFO interface, thus making it easy to trap sufficient holes in only 20 ms.

To evaluate the charge storage stabilities of the two OFET memories, the bias stress characteristics were performed under dark and are shown in Figure 4c. Compared to the OFF currents (programmed state), the ON currents (erased state) of the two OFET memories exhibited more rapid degradation. In this case, the ON/OFF current ratio of the β-PFO device could be maintained over ~10^3 when the stress time was more than 8000 s, 2 times than the amorphous PFO device (4148 s), further confirming that the trapped photogenerated electrons in the β-PFO electret layer were more stable than those in the amorphous one.

Content Effect of β-Phase on the Memory Performances. The effect of β-phase content on the memory performances of pentacene-based OFET memories was also investigated. Higher-content β-phase electrets with similar thickness (60 ± 5 nm) were prepared via spin-coating from toluene and DCE solution,[28] denoted as β-PFO (medium) and β-PFO (high) film, respectively. The content of β-phase can be defined from the excited PL (PLE) spectra with an increasing density peaking at 436 nm (Figure S6), indicating the content followed the order of DCE > toluene > $CHCl_3$. The hole trapping capacities of OFET memories with higher-content β-PFO electrets were characterized as shown in Figure S7. All the memory devices displayed linear increase in ΔV_{TH} as a function of V_{GS}; however, the device with the highest content of β-phase did not show the largest ΔV_{TH}, meaning the hole trapping capability was not consistent with the increasing trend of β-phase content. It was because the high content of β-phase induced harmful surface fluctuation and poor crystallinity of pentacene. Large amounts of traps distributed not only in PFO film but also in the disordered pentacene structure,[32,47] leading to insufficient light erasing and thus a smaller memory window. In addition, the bias stress characteristics of the OFET memories with increasing content of β-phase are displayed in Figure S8. One can see that the memory device with higher content of β-phase had slower degradation, which was mainly caused by the strong electron trapping ability of β-phase.

According to the above analysis, we proposed the potential electrical programming and light erasing mechanism, as shown in Figure 5. When an appropriate negative V_{GS} was applied to

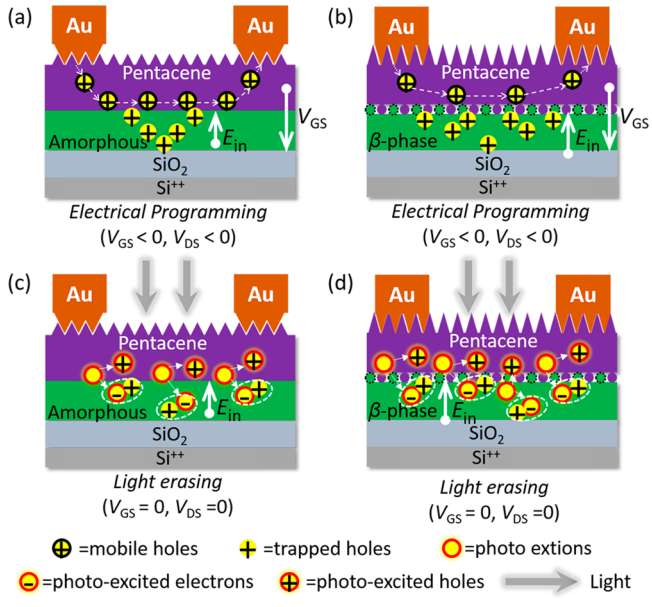

Figure 5. Operational mechanisms of pentacene-based OFET memories operated in electrical programming mode: (a) with amorphous PFO electret; (b) with β-PFO electret. Operational mechanisms of pentacene-based OFET memories operated in light erasing mode: (c) with amorphous PFO electret; (d) with β-PFO electret.

DOI: 10.1021/acsami.6b03792
ACS Appl. Mater. Interfaces XXXX, XXX, XXX−XXX

the OFET memories under dark (Figures 5a and 5b), holes were tunneled from pentacene and trapped into the pentacene/PFO interface and the PFO bulk. Considering the amorphous and β-phase PFO have the same HOMO levels which means the same tunneling barrier, the higher hole trapping capacity of β-phase device is attributed to the self-doped nanostructures for two factors: in one aspect, the self-doped nanostructures provide more charge trapping sites and stronger charge trapping ability at the pentacene/β-PFO interface; in another, the self-doped nanostructures create a larger interfacial contact and thus broaden the tunneling area. The trapped holes would reduce the concentration of holes in the conductive channel and form the internal electric field (E_{in}) which pointed toward pentacene; thus, the transfer curve of the OFET memories shifts to the negative direction. Besides, the injected holes which diffused and were trapped to the SiO_2 interface should also be considered. Control devices with the structure of Si^{2+}/SiO_2/OTS/amorphous or β-PFO/pentacene/Au source−drain have been carried out (Figure S9). A negligible degradation of memory window implied that the trapping at SiO_2 interface existed but played a minor role, especially for a 60 nm thick PFO bulk. When the OFET memory devices are illuminated (Figures 5c and 5d), a large number of photoexcitons are generated in the pentacene layer and minority excitons in the β-PFO layer. Driven by E_{in}, these excitons are quickly divided into photogenerated holes and electrons.[41,43] Photogenerated holes drift toward the conductive channel to form a photocurrent and decreased the electron injection barrier,[19,48] whereas the downward moving photogenerated electrons recombined with most of the trapped holes at the pentacene/PFO interface. As the light illumination time increased, the photogenerated high-energy electrons further diffused into the PFO bulk to neutralize the residual holes; thus, a light-assisted erasing operation was obtained.

CONCLUSION

In summary, synergistic effects of self-doped PFO nanostructures as charge trapping elements were investigated in OFET memories. Compared to amorphous PFO film, the β-PFO layer contains self-doped nanostructures and can be regarded as a "2 in 1" electret, combining merits of simple solution-processed "host−guest" polymeric and nanofloating gate electrets. This special electret has the following significant advantages: (i) self-doped nanostructures to provide more trapping sites and stronger trapping ability; (ii) an enlarged interfacial contact between the initial monolayers of pentacene and β-PFO film to broaden the effective tunneling area; (iii) an additional absorption peak at 437 nm to enhance the photosensitivity of pentacene-based OFET in blue light range (435−450 nm); (iv) the increased hydrophobicity to ensure the stabilities and reliabilities of OFET memories in ambient air; (v) a lower LUMO energy level to provide strong electron trapping ability. Benefiting from the above synergistic effects, the OFET memory based on β-phase PFO as the charge trapping element exhibited impressive memory and photosensitive performances compared with the amorphous one. Our results demonstrated that polymer conformation modulation could be a promising strategy to design novel optoelectronic applications with memory functionality, such as intelligent RFID, optical data encryption, etc.

ASSOCIATED CONTENT

Supporting Information

The Supporting Information is available free of charge on the ACS Publications website at DOI: 10.1021/acsami.6b03792.

Emission spectra of LED, electrical curves of pentacene-based OFET memories with various content of β-phase PFO electrets (PDF)

AUTHOR INFORMATION

Corresponding Authors

*E-mail: iammdyi@njupt.edu.cn (M.Y.).
*E-mail: iamlhxie@njupt.edu.cn (L.X.).
*E-mail: wei-huang@njtech.edu.cn (W.H.).

Author Contributions

⊥Haifeng Ling and Jinyi Lin contributed equally.

Notes

The authors declare no competing financial interest.

ACKNOWLEDGMENTS

The project was supported by the National Basic Research Program of China (2014CB648300, 2015CB932200), National Natural Science Foundation of China (61475074, 21274064, 21504041, 61136003), National Natural Science Funds for Excellent Young Scholar (21322402), Changjiang Scholars and Innovative Research Team in University (IRT_15R37), Natural Science Foundation of Jiangsu Province (BM2012010), Synergetic Innovation Center for Organic Electronics and Information Displays, Excellent Science and Technology Innovation Team of Jiangsu Higher Education Institutions (2013), Natural Science Foundation of Jiangsu Province (14KJB510027), China Postdoctoral Science Foundation (2015M580419), Priority Academic Program Development of Jiangsu Higher Education Institutions (PAPD, YX03001), and Program for Postgraduates Research Innovation in University of Jiangsu Province (KYLX15_0850).

REFERENCES

(1) Heremans, P.; Gelinck, G. H.; Müller, R.; Baeg, K.-J.; Kim, D.-Y.; Noh, Y.-Y. Polymer and Organic Nonvolatile Memory Devices. *Chem. Mater.* **2010**, *23*, 341−358.

(2) Guo, Y.; Yu, G.; Liu, Y. Functional Organic Field-Effect Transistors. *Adv. Mater.* **2010**, *22*, 4427−4447.

(3) Chou, Y.-H.; Chang, H.-C.; Liu, C.-L.; Chen, W.-C. Polymeric Charge Storage Electrets for Non-Volatile Organic Field Effect Transistor Memory Devices. *Polym. Chem.* **2015**, *6*, 341−352.

(4) Han, S.-T.; Zhou, Y.; Roy, V. A. L. Towards the Development of Flexible Non-Volatile Memories. *Adv. Mater.* **2013**, *25*, 5425−5449.

(5) Leong, W. L.; Mathews, N.; Tan, B.; Vaidyanathan, S.; Dotz, F.; Mhaisalkar, S. Towards Printable Organic Thin Film Transistor Based Flash Memory Devices. *J. Mater. Chem.* **2011**, *21*, 5203−5214.

(6) Kang, M.; Baeg, K.-J.; Khim, D.; Noh, Y.-Y.; Kim, D.-Y. Printed, Flexible, Organic Nano-Floating-Gate Memory: Effects of Metal Nanoparticles and Blocking Dielectrics on Memory Characteristics. *Adv. Funct. Mater.* **2013**, *23*, 3503−3512.

(7) Han, S.-T.; Zhou, Y.; Xu, Z.-X.; Huang, L.-B.; Yang, X.-B.; Roy, V. A. L. Microcontact Printing of Ultrahigh Density Gold Nanoparticle Monolayer for Flexible Flash Memories. *Adv. Mater.* **2012**, *24*, 3556−3561.

(8) Baeg, K.-J.; Khim, D.; Kim, J.; Yang, B.-D.; Kang, M.; Jung, S.-W.; You, I.-K.; Kim, D.-Y.; Noh, Y.-Y. High-Performance Top-Gated Organic Field-Effect Transistor Memory Using Electrets for Monolithic Printed Flexible Nand Flash Memory. *Adv. Funct. Mater.* **2012**, *22*, 2915−2926.

DOI: 10.1021/acsami.6b03792
ACS Appl. Mater. Interfaces XXXX, XXX, XXX−XXX

(9) Li, J.; Yan, F. Solution-Processable Low-Voltage and Flexible Floating-Gate Memories Based on an N-Type Polymer Semiconductor and High-K Polymer Gate Dielectrics. *ACS Appl. Mater. Interfaces* **2014**, *6*, 12815−12820.
(10) Han, S. T.; Zhou, Y.; Chen, B.; Zhou, L.; Yan, Y.; Zhang, H.; Roy, V. A. Two-Dimensional Molybdenum Disulphide Nanosheet-Covered Metal Nanoparticle Array as a Floating Gate in Multi-Functional Flash Memories. *Nanoscale* **2015**, *7*, 17496−17503.
(11) Zhang, J.-Y.; Liu, L.-M.; Su, Y.-J.; Gao, X.; Liu, C.-H.; Liu, J.; Dong, B.; Wang, S.-D. Synergistic Effect in Organic Field-Effect Transistor Nonvolatile Memory Utilizing Bimetal Nanoparticles as Nano-Floating-Gate. *Org. Electron.* **2015**, *25*, 324−328.
(12) Chang, H. C.; Lu, C.; Liu, C. L.; Chen, W. C. Single-Crystal C60 Needle/Cupc Nanoparticle Double Floating-Gate for Low-Voltage Organic Transistors Based Non-Volatile Memory Devices. *Adv. Mater.* **2015**, *27*, 27−33.
(13) Tseng, C. W.; Huang, D. C.; Tao, Y. T. Azobenzene-Functionalized Gold Nanoparticles as Hybrid Double-Floating-Gate in Pentacene Thin-Film Transistors/Memories with Enhanced Response, Retention, and Memory Windows. *ACS Appl. Mater. Interfaces* **2013**, *5*, 9528−9536.
(14) Han, S.-T.; Zhou, Y.; Xu, Z.-X.; Roy, V. A. L.; Hung, T. F. Nanoparticle Size Dependent Threshold Voltage Shifts in Organic Memory Transistors. *J. Mater. Chem.* **2011**, *21*, 14575−14580.
(15) She, X.-J.; Liu, C.-H.; Sun, Q.-J.; Gao, X.; Wang, S.-D. Morphology Control of Tunneling Dielectric Towards High-Performance Organic Field-Effect Transistor Nonvolatile Memory. *Org. Electron.* **2012**, *13*, 1908−1915.
(16) Wang, W.; Hwang, S. K.; Kim, K. L.; Lee, J. H.; Cho, S. M.; Park, C. Highly Reliable Top-Gated Thin-Film Transistor Memory with Semiconducting, Tunneling, Charge-Trapping, and Blocking Layers All of Flexible Polymers. *ACS Appl. Mater. Interfaces* **2015**, *7*, 10957−10965.
(17) Mukherjee, B.; Mukherjee, M.; Choi, Y.; Pyo, S. Control over Multifunctionality in Optoelectronic Device Based on Organic Phototransistor. *ACS Appl. Mater. Interfaces* **2010**, *2*, 1614−1620.
(18) Lin, J.; Li, W.; Yu, Z.; Yi, M.; Ling, H.; Xie, L.; Li, S.; Huang, W. π-Conjugation-Interrupted Hyperbranched Polymer Electrets for Organic Nonvolatile Transistor Memory Devices. *J. Mater. Chem. C* **2014**, *2*, 3738−3743.
(19) Yi, M.; Xie, M.; Shao, Y.; Li, W.; Ling, H.; Xie, L.; Yang, T.; Fan, Q.; Zhu, J.; Huang, W. Light Programmable/Erasable Organic Field-Effect Transistor Ambipolar Memory Devices Based on the Pentacene/PVK Active Layer. *J. Mater. Chem. C* **2015**, *3*, 5220−5225.
(20) Sun, C.; Lin, Z.; Xu, W.; Xie, L.; Ling, H.; Chen, M.; Wang, J.; Wei, Y.; Yi, M.; Huang, W. Dipole Moment Effect of Cyano-Substituted Spirofluorenes on Charge Storage for Organic Transistor Memory. *J. Phys. Chem. C* **2015**, *119*, 18014−18021.
(21) Gao, X.; Liu, C.-H.; She, X.-J.; Li, Q.-L.; Liu, J.; Wang, S.-D. Photon-Energy-Dependent Light Effects in Organic Nano-Floating-Gate Nonvolatile Memories. *Org. Electron.* **2014**, *15*, 2486−2491.
(22) Perevedentsev, A.; Sonnefraud, Y.; Belton, C. R.; Sharma, S.; Cass, A. E.; Maier, S. A.; Kim, J. S.; Stavrinou, P. N.; Bradley, D. D. Dip-Pen Patterning of Poly(9,9-Dioctylfluorene) Chain-Conformation-Based Nano-Photonic Elements. *Nat. Commun.* **2015**, *6*, 5977.
(23) Ryu, G.; Stavrinou, P. N.; Bradley, D. D. C. Spatial Patterning of the β-Phase in Poly(9,9-Dioctylfluorene): A Metamaterials-Inspired Molecular Conformation Approach to the Fabrication of Polymer Semiconductor Optical Structures. *Adv. Funct. Mater.* **2009**, *19*, 3237−3242.
(24) Zhang, X. W.; Hu, Q.; Lin, J. Y.; Lei, Z. F.; Guo, X.; Xie, L. H.; Lai, W. Y.; Huang, W. Efficient and Stable Deep Blue Polymer Light-Emitting Devices Based on Beta-Phase Poly(9,9-Dioctylfluorene). *Appl. Phys. Lett.* **2013**, *103*, 153301.
(25) Lu, H. H.; Liu, C. Y.; Chang, C. H.; Chen, S. A. Self-Dopant Formation in Poly(9,9-dioctylfluorene) Via a Dipping Method for Efficient and Stable Pure-Blue Electroluminescence. *Adv. Mater.* **2007**, *19*, 2574−2579.
(26) Shih, C.-C.; Chiu, Y.-C.; Lee, W.-Y.; Chen, J.-Y.; Chen, W.-C. Conjugated Polymer Nanoparticles as Nano Floating Gate Electrets for High Performance Nonvolatile Organic Transistor Memory Devices. *Adv. Funct. Mater.* **2015**, *25*, 1511−1519.
(27) Feng, C.; Mei, T.; Hu, X.; Pavel, N. A Pentacene Field-Effect Transistor with Light-Programmable Threshold Voltage. *Org. Electron.* **2010**, *11*, 1713−1718.
(28) Lin, Z.-Q.; Shi, N.-E.; Li, Y.-B.; Qiu, D.; Zhang, L.; Lin, J.-Y.; Zhao, J.-F.; Wang, C.; Xie, L.-H.; Huang, W. Preparation and Characterization of Polyfluorene-Based Supramolecular π-Conjugated Polymer Gels. *J. Phys. Chem. C* **2011**, *115*, 4418−4424.
(29) Yang, S. Y.; Shin, K.; Park, C. E. The Effect of Gate-Dielectric Surface Energy on Pentacene Morphology and Organic Field-Effect Transistor Characteristics. *Adv. Funct. Mater.* **2005**, *15*, 1806−1814.
(30) Kim, K.; Hahm, S. G.; Kim, Y.; Kim, S.; Kim, S. H.; Park, C. E. Realization of Electrically Stable Organic Field-Effect Transistors Using Simple Polymer Blended Dielectrics. *Org. Electron.* **2015**, *21*, 111−116.
(31) Kim, S. H.; Jang, M.; Yang, H.; Park, C. E. Effect of Pentacene-Dielectric Affinity on Pentacene Thin Film Growth Morphology in Organic Field-Effect Transistors. *J. Mater. Chem.* **2010**, *20*, 5612−5620.
(32) Min, H.-G.; Seo, E.; Lee, J.; Park, N.; Lee, H. S. Behavior of Pentacene Molecules Deposited onto Roughness-Controlled Polymer Dielectrics Films and Its Effect on Fet Performance. *Synth. Met.* **2013**, *163*, 7−12.
(33) Kim, D. H.; Lee, H. S.; Yang, H. C.; Yang, L.; Cho, K. Tunable Crystal Nanostructures of Pentacene Thin Films on Gate Dielectrics Possessing Surface-Order Control. *Adv. Funct. Mater.* **2008**, *18*, 1363−1370.
(34) Ma, N.; Jena, D. Charge Scattering and Mobility in Atomically Thin Semiconductors. *Phys. Rev. X* **2014**, *4*, 011043.
(35) Hwang, D. K.; Oh, M. S.; Hwang, J. M.; Kim, J. H.; Im, S. Hysteresis Mechanisms of Pentacene Thin-Film Transistors with Polymer/Oxide Bilayer Gate Dielectrics. *Appl. Phys. Lett.* **2008**, *92*, 013304.
(36) Gu, G.; Kane, M. G.; Doty, J. E.; Firester, A. H. Electron Traps and Hysteresis in Pentacene-Based Organic Thin-Film Transistors. *Appl. Phys. Lett.* **2005**, *87*, 243512.
(37) Qu, M.; Li, H.; Liu, R.; Zhang, S. L.; Qiu, Z. J. Interaction of Bipolaron with the H_2O/O_2 Redox Couple Causes Current Hysteresis in Organic Thin-Film Transistors. *Nat. Commun.* **2014**, *5*, 3185.
(38) Park, J.; Do, L.-M.; Bae, J.-H.; Jeong, Y.-S.; Pearson, C.; Petty, M. C. Environmental Effects on the Electrical Behavior of Pentacene Thin-Film Transistors with a Poly(Methyl Methacrylate) Gate Insulator. *Org. Electron.* **2013**, *14*, 2101−2107.
(39) Kim, S. H.; Yang, H.; Yang, S. Y.; Hong, K.; Choi, D.; Yang, C.; Chung, D. S.; Park, C. E. Effect of Water in Ambient Air on Hysteresis in Pentacene Field-Effect Transistors Containing Gate Dielectrics Coated with Polymers with Different Functional Groups. *Org. Electron.* **2008**, *9*, 673−677.
(40) Wang, J.; Wang, X.; Xu, W. J.; Xie, L. H.; Liu, Y. Y.; Yi, M. D.; Huang, W. Detection of Trapped Charges in the Blend Films of Polystyrene/SFDBAO Electrets by Electrostatic and Kelvin Probe Force Microscopy. *Phys. Chem. Chem. Phys.* **2016**, *18*, 9412−9418.
(41) Yi, M.; Shu, J.; Wang, Y.; Ling, H.; Song, C.; Li, W.; Xie, L.; Huang, W. The Effect of Porous Structure of Pmma Tunneling Dielectric Layer on the Performance of Nonvolatile Floating-Gate Organic Field-Effect Transistor Memory Devices. *Org. Electron.* **2016**, *33*, 95−101.
(42) Li, W.; Yi, M.; Ling, H.; Guo, F.; Wang, T.; Yang, T.; Xie, L.; Huang, W. Analysis of Temperature-Dependent Electrical Transport Properties of Nonvolatile Organic Field-Effect Transistor Memories Based on Pmma Film as Charge Trapping Layer. *J. Phys. D: Appl. Phys.* **2016**, *49*, 125104.
(43) Han, S.-T.; Zhou, Y.; Zhou, L.; Yan, Y.; Huang, L.-B.; Wu, W.; Roy, V. A. L. Cdse/Zns Core-Shell Quantum Dots Charge Trapping Layer for Flexible Photonic Memory. *J. Mater. Chem. C* **2015**, *3*, 3173−3180.

DOI: 10.1021/acsami.6b03792
ACS Appl. Mater. Interfaces XXXX, XXX, XXX−XXX

(44) Guo, Y.; Di, C.-A.; Ye, S.; Sun, X.; Zheng, J.; Wen, Y.; Wu, W.; Yu, G.; Liu, Y. Multibit Storage of Organic Thin-Film Field-Effect Transistors. *Adv. Mater.* **2009**, *21*, 1954−1959.
(45) Shih, C. C.; Lee, W. Y.; Chiu, Y. C.; Hsu, H. W.; Chang, H. C.; Liu, C. L.; Chen, W. C. High Performance Transparent Transistor Memory Devices Using Nano-Floating Gate of Polymer/Zno Nanocomposites. *Sci. Rep.* **2016**, *6*, 20129.
(46) Debucquoy, M.; Rockelé, M.; Genoe, J.; Gelinck, G. H.; Heremans, P. Charge Trapping in Organic Transistor Memories: On the Role of Electrons and Holes. *Org. Electron.* **2009**, *10*, 1252−1258.
(47) Han, C. Y.; Tang, W. M.; Leung, C. H.; Che, C. M.; Lai, P. T. High-Mobility Pentacene Thin-Film Transistor by Using Laxta(1−X)Oy as Gate Dielectric. *Org. Electron.* **2014**, *15*, 2499−2504.
(48) Du, L.; Luo, X.; Lv, W.; Zhao, F.; Peng, Y.; Tang, Y.; Wang, Y. High-Performance Organic Broadband Photomemory Transistors Exhibiting Remarkable Uv-Nir Response. *Phys. Chem. Chem. Phys.* **2016**, *18*, 13108−13117.

DOI: 10.1021/acsami.6b03792
ACS Appl. Mater. Interfaces XXXX, XXX, XXX−XXX